

# Validation of a Simulation Environment for Future Space Traffic Management

Alaric C. Gregoire\* and Brian C. Gunter†

*Daniel Guggenheim School of Aerospace Engineering, Georgia Institute of Technology, Atlanta, GA, 30332*

Mariel Borowitz‡

*Sam Nunn School of International Affairs, Georgia Institute of Technology, Atlanta, GA, 30332-0610*

Lauri K. Newman§

*Conjunction Assessment Risk Analysis Program Officer, NASA Headquarters, Science Mission Directorate,*

Gerald A. Schweiger¶

*Daniel Guggenheim School of Aerospace Engineering, Georgia Institute of Technology, Atlanta, GA, 30332*

This study presents initial results of a newly developed simulation environment intended to explore and assess future Space Traffic Management (STM) scenarios. The number of new Resident Space Objects (RSOs) in near-Earth orbit is expected to increase significantly with the expected future deployment of a number of large constellations. These future scenarios involve the addition of many tens of thousands of new RSOs, making the analysis into their impact on collision risk extend beyond what traditional data-mining of present-day conjunction data can reliably predict. To address this, a robust simulation environment was developed that implements a full force-model for orbit propagation, and computes continuous all-on-all conjunction statistics for arbitrarily large catalog sizes and simulation timeframes. Collision avoidance and station-keeping maneuvers can be optionally implemented based on configurable user inputs including physical characteristics and spacecraft meta-data (e.g., commercial/government, owner country, etc.). Constellation build-out and de-orbit scenarios were also implemented and modeled based on real-data analysis. Validation of the simulation results was a critical component of the simulation development, and was done using the current catalog with comparisons against both public and internal NASA data-sets. The comparisons demonstrate that, with the appropriate settings, representative levels of conjunction rates and probabilities can be obtained, providing confidence that the simulation tool can generate meaningful outcomes for test scenarios. As an initial demonstration of the tool's capabilities, year-long simulations with station-keeping were conducted to examine conjunction histories using both the current object catalog (5800 active satellites) and a hypothetical 60,000 object scenario involving five potential large constellations. Output metrics include the number of conjunction events, estimates of collision consequence (fragmentation), delta-V maneuver costs, and the probability of at least one collision occurring. The results highlight the potential that the simulation tool has for incorporating and running performance comparisons between, e.g., various sets of maneuver guidelines, industry norms, and definitions of risk, with the overall objective of providing actionable data to STM policy makers. The presentation will provide an overview of the simulation development and validation efforts, as well as a discussion of observations gathered from the initial simulations performed.

## I. Nomenclature

---

\*PhD Candidate, [agregoire3@gatech.edu](mailto:agregoire3@gatech.edu), AIAA Student Member

† Associate Professor, AIAA Associate Fellow

‡ Associate Professor

§ Conjunction Assessment Program Officer, AIAA Associate Fellow

¶ Graduate Research Assistant, AIAA Student Member

$a$	=	Keplerian semimajor axis
$C$	=	Covariance matrix
$cr$	=	Combined hard body conjunction radius
$E$	=	Keplerian eccentric anomaly
$e$	=	Keplerian eccentricity
$DU$	=	Canonical distance unit
$L_c$	=	Characteristic Length
$M$	=	Keplerian mean anomaly
$N$	=	Number of samples
$n$	=	Keplerian mean motion
$r$	=	Orbital radius
$T$	=	Orbital period
$TU$	=	Canonical time unit
$\delta t$	=	time-step
$t_{drift}$	=	Time required for maneuver
$t_{raise}$	=	Time required to raise orbital altitude
$V$	=	Satellite velocity
$V_r$	=	Relative satellite velocity
$\Delta v_I$	=	Satellite velocity change in in-track direction
$xm$	=	Miss distance in the $x$ direction
$ym$	=	Miss distance in the $y$ direction
$v$	=	Keplerian true anomaly
$\mu$	=	Earth gravitational parameter
$\chi$	=	Satellite state estimate residual
$\sigma_x$	=	Standard deviation of uncertainty in the $x$ direction
$\sigma_y$	=	Standard deviation of uncertainty in the $y$ direction

## II. Introduction

THE resident space object (RSO) population is expected to see significant growth in the coming decade, with the number of approved and proposed constellations necessitating a paradigm shift in how Space Traffic Management (STM) is introduced, assessed, and implemented. While independent operator groups have made best practice guidelines for STM, these are often limited in participation and in scale.[1] To sustain the use of space for the variety of scientific and economic operations envisioned, a coordinated effort is essential to assess efficient collision avoidance behaviors and mitigation strategies. This includes defining how risk is determined, the threshold for a dangerous and actionable situation, and what types of actions should be taken. As an illustration, Figure 1 depicts just a few recently accepted constellation FCC filings, and highlights the overlap of orbit regimes and potential for high-density regions of space. In an effort to enable an examination of the effectiveness of particular mitigation strategies in a variety of possible space environments, a simulation environment was created with a broad number of input settings and capabilities. More details of the simulation environment will be discussed later, but in short the tool builds on earlier efforts [2, 3] to incorporate a full force-model for orbit propagation, and computes continuous all-on-all conjunction statistics for arbitrarily large catalog sizes and simulation timeframes. This permits the exploration of a range of STM concepts, such as new maneuver strategies, observation tracking requirements, and the influence of inter-operator cooperation and communication. Simulation is the natural choice for such large and complex scenarios, especially given that data-mining historical observational data sets cannot be reliably extrapolated to a future in which the location and density of RSOs will be so dramatically different than present-day.

The development of the simulations took into consideration a number of key aspects, such as fidelity, computational efficiency, and validation. It was paramount that the simulation environment produce output representative of the truth if the tool is to be used to develop and experiment with new STM strategies. The goal was not to exactly reproduce reality, which is difficult to do beyond a few days even with state-of-the-art time-varying gravity, atmospheric and radiation pressure models, but to incorporate enough fidelity in the dynamics to make the analysis tractable computationally, but also such that the aggregate statistics over days and weeks are on par with those seen from real-data comparisons. Validation of these statistics was performed through comparisons against various data sets, such as those available from

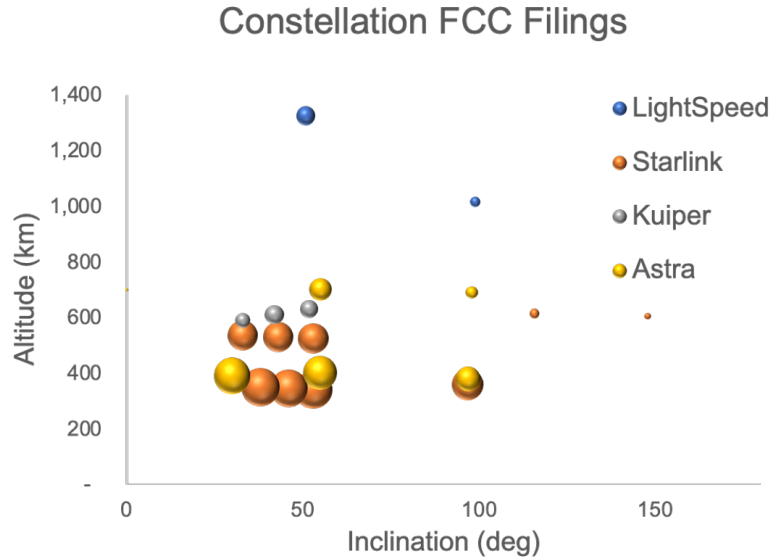


**Fig. 1 Planned Constellation Design Locations**

Celestrak \*, which offers a public conjunction service for public catalogs for a week at a time. Celestrak creates a forecast of conjunctions for active payloads screened against all public objects in orbit using data provided by the 18th Space Defense Squadron (SDS). When used as a verification source in later in this paper, the environment reproduces a similar number of short-term encounters and distribution of risk magnitudes. Internal data provided by NASA’s Conjunction Assessment Risk Analysis (CARA) group covers nearly a year of historical encounters for NASA assets as well as a more complete satellite catalog with best-estimate satellite radii. Archive access enables long-term trends to be isolated and understood. Further examination of the augmented catalog for validation purposes is continued in Section IV.B.

In addition to direct comparisons to conjunction rates, effort was taken to replicate the behaviors of two well-established constellations, Starlink and OneWeb, in terms of station keeping, orbit raising, satellite retirement, maneuver lead-time, and risk tolerance. In particular, data-mined maneuvers for orbit raising, station keeping, and end-of-life de-orbiting were derived directly from two-line element (TLE) data set histories for these large constellations. By replicating the practices of two unique constellations, the models to represent these constellations are written in a more generalized way and become easier to implement for other scenarios. Simulating orbit raising, station keeping, and de-orbiting are the next step in terms of evaluating simulation realism and the relevance of its output, as the propagation of constellation satellites using only Keplerian dynamics does not represent industry practice. For example, many of the major constellation operators conduct high-cadence orbit maintenance maneuvers that can be combined with avoidance strategies, which our simulation tool can emulate.

The simulation environment provides the flexibility for operator-specific parameters, which are implemented as input definitions and satellite meta-data. Input definitions include basic settings such as the initial satellite population and distribution, a start and end epoch, acceptable risk thresholds for collision avoidance, and the search volume used. Maneuver strategies can also be tailored to an individual constellation, or be performed based on a set of standardized rules determined from the satellite meta-data. This satellite meta-data is the combination of various spacecraft attributes, such as country ownership, maneuverability, operational status, age, mass, usage type, whether or not the satellite is a member of a constellation, or simply the context in terms of orbital dynamics. All of these attributes are assigned at the start of a simulation, but the maneuver burden definition is applied by prioritizing of one of these attributes (e.g. the satellite with the lower mass maneuvers) or a custom combination in a weighted cost function. For the case of two active satellites, both satellites may share the burden to reduce the individual cost, though this does not necessarily reduce the cost upon the population as a whole. Country of origin and owner-type designations allows the exploration of collision avoidance responsibility across government, scientific, and commercial operators.

\*[www.celestrak.com](http://www.celestrak.com)

Once operationally relevant inputs are supplied, equally relevant outputs are tracked. Overall, the outputs shine a light on the operational, financial, and environmental burdens for a scenario. Each encounter documents the miss distance, relative velocity, date, probability of collision ( $P_c$ ), debris count that would arise from a collision (fragmentation), and satellite IDs. This allows a detailed look at all predictions for trend detection and verification. Summary statistics are compiled for high-level comparisons such as the number of events at varying probabilities of collision, the number of early warning notifications, inter-constellation vs. intra-constellation events, and additional events constellations impose on other active satellites. Event frequency is a commonly used output metric for risk assessment, but this is insufficient for a simulation of the future where collision avoidance maneuvers are possible. The change in velocity required along with the number of maneuvers executed is recorded for each satellite. Additionally, a list of satellite IDs that will decay during a simulation provides insight into the effectiveness of de-orbit strategies. The encounter frequency gives insight into the overall collision risk of a space population, while the change in velocity (i.e.,  $\Delta V$ ) is a proxy for the financial burden of propulsive maneuvers. In the interest of describing overall space sustainability, the total likelihood of at least one collision occurring during the simulation is reported along with the number of debris objects that would be created from catastrophic collisions.[4][5] If the the total collision probability approaches unity, the number of identified collisions is incremented. This tracks the total number of collisions for longer simulated time-spans.

Data-mining is often used to compare the probability algorithms and maneuver methodologies to derive optimized solution for future encounters; however, data-mining can only be utilized when extrapolated to similar scenarios. The size of current operational constellations is small relative to the anticipated number and density of proposed future systems. Even Starlink, with thousands of deployed assets currently on orbit, is only a fraction of its full operational design of 13,000+ satellites, and the intersection of dense constellations has yet to occur in Low Earth Orbit. As such, the simulation environment developed through this study should serve as a valuable way to realistically model this future space environment and ideally provide insight and potential guidance on how to have a high density of RSOs from global operators interact with minimal impact on operations.

Tracking the conjunction history of hundreds of thousands of RSOs and making the associated trajectory adjustments over months and years posed a sizeable technical challenge from a computational perspective. Leveraging high-performance computing platforms, and various data processing and programming efficiencies, the simulation tool is able to handle large object catalogs (250,000+ objects) on relatively modest compute platforms (e.g., 24-core processor node, with 8 Gb of memory), with run times of under one day for a typical year-long simulation run. This enables the submission of multiple concurrent simulations using compute clusters common to most academic and research institutions, or the possibility of running larger catalogs over longer periods.

Other frameworks have been introduced to compute all-on-all types of conjunction analyses[6], including the consideration of hypothetical constellations. A framework developed by the Technical University of Darmstadt has produced a model that also implements orbit-raising, station keeping, and end-of-life called “Rules4CREAM” (R4C), and while the importance of orbit-raising methods are mentioned, only collision detection is currently output by the framework. Alternatively, the simulation framework presented here expands beyond collision detection to collision avoidance comparisons, examinations of acceptable risk, and the analysis of context-based maneuver assignment, all in a dynamic space population. [7][8] These outputs enable satellite operators and policy makers to compare the relative efficiency between various sets of proposed regulations, risk calculations and definitions, and the assumed satellite population. To highlight the capabilities and potential of the new simulation tool, a pair of representative use-cases are explored. The first is a propagation of the current catalog of active satellites, comprising approximately 5800 objects. The rates of active-on-active and active-on-debris is summarized, and compared to other recent studies in the literature. Second, a hypothetical scenario is explored in which a collection of large constellations likely to reach orbit in the next decade are then added to the space environment. The determination of which constellations to include was derived from a parallel study [REF SciTech paper], but incorporated a number of metrics such as FCC filings, publicly announced funding, prior demonstration launches, and more. This resulted in approximately over 60,000 new RSOs from 5 of the largest potential new constellation operators. Sample case studies using these constellations are summarized and compared in Section VI to highlight some of the anticipated trends and identify aspects that require additional study.

### III. Simulation Overview

For a given simulation time-frame, checks for collision detection can be generated at user-defined intervals; however, testing has shown that an interval of two minutes strikes a good balance between fidelity and computational efficiency. At these two-minute time-steps, a series of filters are used to narrow down which satellites pass within a specified screening volume over a given time window (e.g., 72 hours). Following a near-miss, the  $P_c$  of the conjunction is

modeled using either a high or low relative velocity approach. Conjunctions containing only debris are optionally ignored as they are not actionable, but can be included as part of fragmentation assessments. Active satellites have their notification count incremented by one to track the Owner/Operator (O/O) workload. Typical notification timelines may be three or more days in advance, and although data approaching the encounter may remove the maneuver burden for operators in practice, the implementation of a time-varying covariance model is on-going. When a predicted encounter is at an actionable  $P_c$ , a maneuver is executed using the priority metrics specified by the input guidelines. The definition of what is deemed actionable is a locally set value, but is typically in the range of  $P_c \geq 1E-04$ [9]. The collision detection workflow initially resembled that of the "Smart Sieve" [10] and builds off the experiences of previous software versions. [2] The first filter is called the periapsis test and determines if two orbits geometrically intersect, eliminating near-circular orbits with different altitudes. The next three filters use increasingly finer interpolation of the relative satellite position magnitude compared to the volume threshold. Finally, propagation is employed to determine the true radial distance at the Time of Closest Approach (TCA).

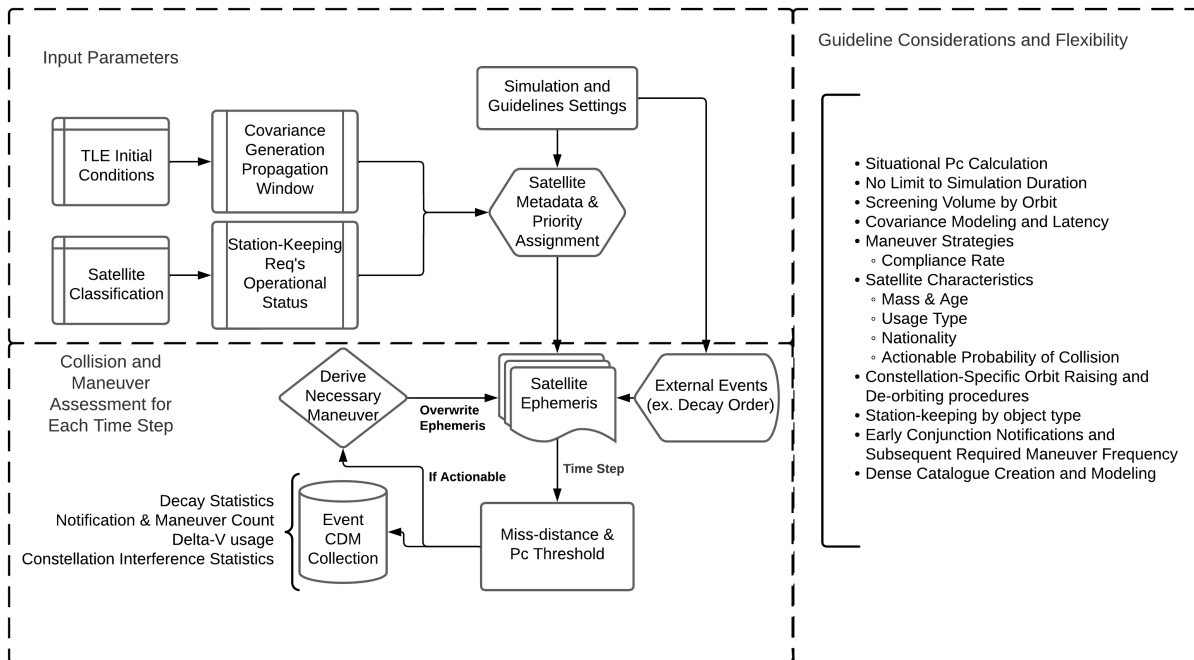


**Fig. 2 Simulation Framework Flowchart.**

As shown in Figure 2, for every encounter exceeding the defined risk threshold, the framework collects a variety of contextual information to output including a record of decayed satellites, the number of early-warning notifications, subsequent maneuvers, and the sum of all required velocity changes. Beyond modeling the dynamics of future space populations, transient satellite obstructions are tracked for constellation orbit raising and decay strategies, and the frequency of inter-constellation events to assess the conflict of proposed and existing constellations.

### A. Propagator

The Simplified General Perturbations (SGP4) propagator uses simplified solar, atmospheric, and gravitational perturbations and is designed specifically for use with Two Line Element Sets (TLEs). Although SGP4 is not the highest fidelity propagator available, reproducing realistic rates of conjunctions was the primary intent for the simulations, which SGP4 provides in a computationally efficient manner. Despite the accumulation of error with time, the physics of the orbits are accurate enough to allow commonly known perturbations like gravitational precession and altitude dependent drag. The initial conditions for future constellations must be created manually based on publicly available reports such as FCC filings. Therefore, the ability of constellation operators to accurately deploy all of their satellites must be assumed. The force modeling within the simulation propagator also requires the use of station keeping to

"freeze" constellation spacecraft within the bounds of designed orbits and protect active satellites from an unrealistic, early decay.

## B. Covariance

TLEs are among the most common method for public satellite data distribution, so they are used for both the creating initial orbit element conditions as well as for estimating position covariance. In the absence of a pre-defined, or apriori, position covariance for a given RSO, the covariance can be initialized by taking the standard deviation of position and velocity estimates taken from a time-series of TLEs that have all been propagated to the same epoch. A single residual is the difference between a propagated TLE state and the most up-to-date trajectories. To compute the covariance, the sum of the residuals is computed for at-most three days of TLE history. The uncertainty in position is not due entirely to un-modeled forces, but also the uncertainty in the ballistic coefficient assumed when making a best fit TLE from orbit determination. The covariance matrix is constructed by multiplying the sum of residuals by its transpose and dividing by the number of samples minus ones, as described in Equations 1 and 2, in this case resulting in a 6x6 matrix for position and velocity. This is the computation of the sample covariance rather than the population covariance. When creating covariance estimates with a TLE history the covariance matrix is static over the length of the simulation in the Earth inertial frame. When converting to reference frames utilized by collision detection algorithms, the covariance is geometrically mapped onto a coordinate triad derived from the instantaneous radial and angular momentum directions. The volume of the ellipsoid in inertial axes is identical in volume to the projection, but typically the uncertainty in the radial direction is an order of magnitude smaller than the other two which increase in length to conserve volume. Thus, the static covariance in Earth-inertial coordinates is dynamic for orbits with non-zero eccentricity, and direction-dependent close approach search thresholds may be applied to reflect operational experience. Concerning the volume of the uncertainty ellipsoid, the covariance is multiplied by a scale factor to equally adjust the magnitude of uncertainty of all axes. The implementation of a scale factor is discussed further in Section IV.B. NASA CARA supplied CDMs for 56 NASA assets, best-estimate satellite radii, and an extended satellite catalog so that the effect of scale factor on predicted encounter frequency can be assessed.

$$\delta X = \sum_{n=1}^N X - X_n \quad (1)$$

$$C = \frac{1}{N-1} E[\delta X \delta X^T] \quad (2)$$

## C. Probability of Collision

The calculation of  $P_c$  can be visually understood as how much two covariance ellipses overlap between two satellites, but this is a three dimensional operation, and a triple integral can become computationally burdensome. Instead, a two dimensional approximation can be applied under the assumption that the covariance matrices are both independent and Gaussian. In addition, the relative velocity of the two objects must be large enough to assume linear motion for the duration of the encounter. This acts as a 2D projection perpendicular to the relative velocity of the true 3D covariance. The projections of the covariance ellipses are referred to as the encounter plane, and the projections for both satellites are summed to create a combined covariance centered on the primary object. This is only possible when the covariance matrices are independent and Gaussian. After this simplification, the probability of collision can be represented as a double integral. The combined hard body radius (HBR), is either known, estimated from the radar cross section of a satellite, or simply assumed to be a default value. [11] A common worst-case assumption is 20-meters, 18.5 meters for the primary and 1.5 meters for the secondary.

Figure 3 depicts the simplification of a three-dimensional covariance into two dimensions using the relative velocity vector.

$$P_c = \frac{1}{2\pi\sigma_x\sigma_y} \int_{-cr}^{cr} \int_{-\sqrt{cr^2-x^2}}^{\sqrt{cr^2-x^2}} e^{-\frac{1}{2}[(\frac{x-x_m}{\sigma_x})^2 + (\frac{y-y_m}{\sigma_y})^2]} dy dx \quad (3)$$

Using Chan's method to simplify this expression, the double integral is approximated by a 1D Rician probability density function (pdf) with an infinite series summation.

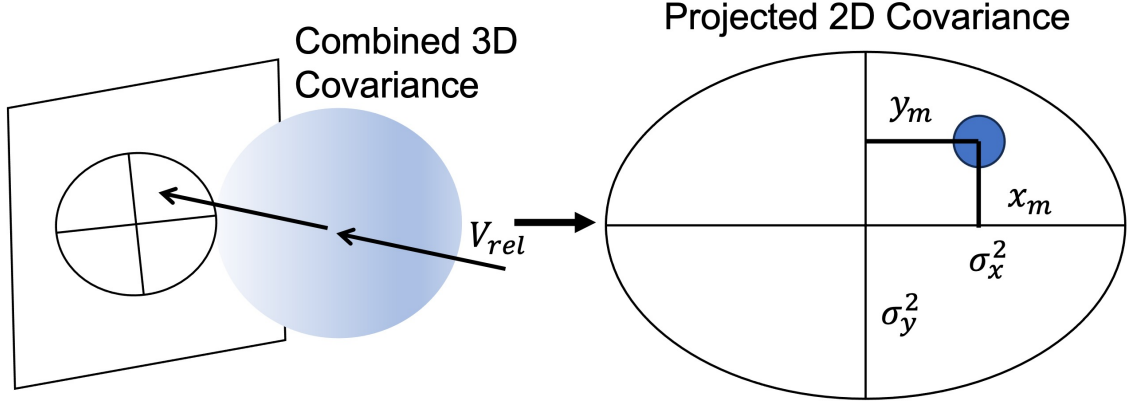


**Fig. 3 Simplification to the Encounter Plane.**

$$Pc = \exp\left(\frac{-v}{2}\right) \sum_{m=0}^{\infty} \left[ \frac{v^m}{(2m)(m!)} \left(1 - \exp\left(\frac{-u}{2}\right) \sum_{k=0}^m \frac{u^k}{(2k)(k!)}\right) \right] \quad (4)$$

$$u = \frac{cr^2}{\sigma_x \sigma_y} \quad (5)$$

$$v = \frac{x_m^2}{\sigma_x^2} + \frac{y_m^2}{\sigma_y^2} \quad (6)$$

In practice, less than 10 iterations of the outer summation converges well for  $Pc > 1E-7$  events, while low speed encounters require removing the linear assumption.[12] This is approached by making miss distance a function of time. [13]

#### D. Fragmentation

Fragmentation refers to creation of debris due to the collision between two objects. The NASA standard breakup model is included in the simulation environment to track consequences of conjunctions in the event that the collision occurred. For mass one defined as the larger of the two, the energy created from a collision is the following.[14]

$$\text{Energy} = \frac{m_2 V_r^2}{2m_1} \quad (7)$$

$$M = \begin{cases} m_1 + m_2, & \text{if Energy} \geq 40000 \text{ joules} \\ \frac{V_r m_2}{1000}, & \text{otherwise} \end{cases} \quad (8)$$

$$\text{Pieces} = \text{round}[0.1M^{0.75} L_c^{-1.71}] \quad (9)$$

This model is created with the assumption that all objects are greater than five-centimeters, so the typical characteristic length is five centimeters in Equation 9.

Simulating the satellite catalog on February 4th, 2023, for one year, some preliminary fragmentation results have been retrieved with a  $Pc$  threshold of  $1E-5$ . No collision avoidance maneuvers were performed to simulate the worst case scenario. Collisions are classically qualified as catastrophic when they exceed 40,000 joules of energy. Relative

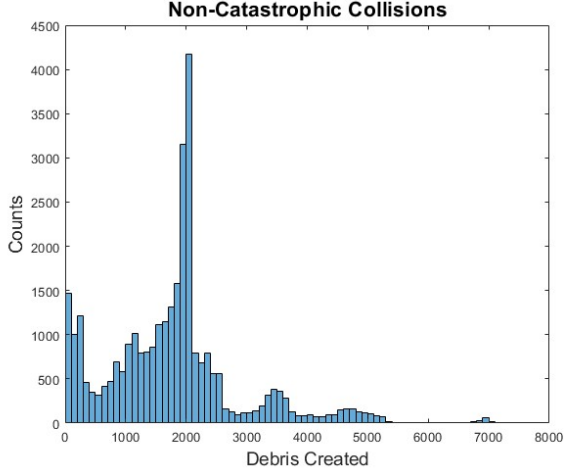


**Fig. 4 Non-Catastrophic Events.**

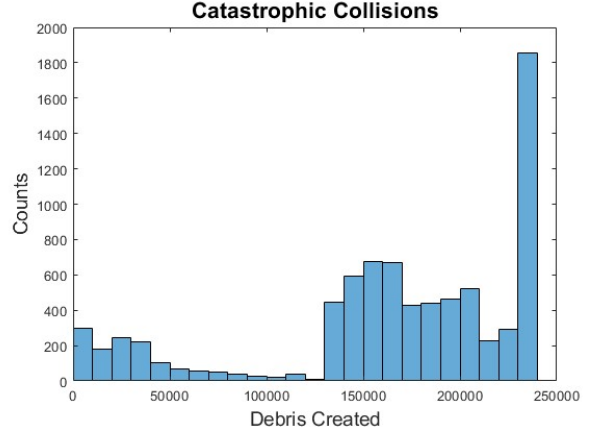


**Fig. 5 Catastrophic Events.**

velocity is the driving characteristic for collision energy, and even relatively small impacting masses produce hundreds of pieces of debris when impacting another 100 kilogram satellite. For future scenarios, the anticipated debris creation for a new constellation can be used to guide the design of satellites and find a balance in acceptable risk. Figure 4 shows the distribution and number of fragments created by the non-catastrophic collisions whose energy is below the threshold of 40,000 joules. This is only eight percent of total events, and this is only representative of collisions between catalogued objects. The estimated volume of objects less than 5 centimeters in size not is represented in the simulation. Of the remaining 92 percent, over half were intra-constellation events, and the relative velocities were so consistent that they were omitted for the readability of Figure 5. With proportion of events classified as catastrophic, the creation of hundreds of thousands of new fragments given a collision is not insignificant. For the special case of no avoidance maneuvers, the simulation revealed that two collisions occurred within 5 standard-deviations of certainty, and 3 at two standard-deviations. Therefore, collision avoidance presents itself as a necessity even with current space populations.

### E. Maneuvers

When an event has been deemed actionable by the simulation, either one or both satellites will undergo a maneuver. The phasing maneuver for a single active satellite begins by determining the orbital period, and then the number of revolutions to epoch.

$$T = 2\pi\sqrt{\frac{a^3}{\mu}} \quad (10)$$

The effect of the maneuver is to change the true anomaly of the satellite by first slightly increasing the orbital period for a number of orbits before conducting a second burn to circularize. The effect of this pair of burns is a change in the true anomaly of the satellite that avoids future conjunctions that may otherwise continue on a cyclical basis. The true anomaly change is depicted in Figure 6.

$$\Delta E = 2 \arctan \left( \sqrt{\frac{1-e}{1+e}} \tan \left( \frac{\nu}{2} \right) \right) \quad (11)$$

Using the desired drift angle, Kepler's equation is used to calculate the time required to drift a given eccentric anomaly over  $N$  orbits. When adding this drift time to the orbital period, the new semi-major axis can be derived using the previous relationship to orbital period, followed by the magnitude of the executed burn magnitude. Because the satellites maneuvers are screened for follow-up collisions, maneuvering satellites do not always successfully return to their orbit. If the first maneuver is possible and the return is not, the return maneuver will be ignored and station-keeping will be responsible for returning the satellite over a longer period of time.

$$t_{drift} = \frac{T}{2\pi} \frac{\Delta E - e \sin \Delta E}{N} \quad (12)$$

$$\Delta V = \sqrt{\mu\left(\frac{2}{r} - \frac{1}{a_{new}}\right)} - V \quad (13)$$

To limit the amount of fuel used, the true anomaly change starts small and is increased if follow-on conjunctions are detected. Specifically, the initial true anomaly is equal to the screening volume divided by the conjunction relative position magnitude. This uses the small angle assumption for arcs and limits the size of screening volume. Iteration continues until a safe maneuver pair is found or the iteration limit is reached. Recognizing that O/Os frequently combine avoidance maneuvers with station keeping, this will likely not be the true optimum for avoidance, but magnitude of velocity changes still has value for comparisons between rule-sets. For the case of two active satellites the process is the

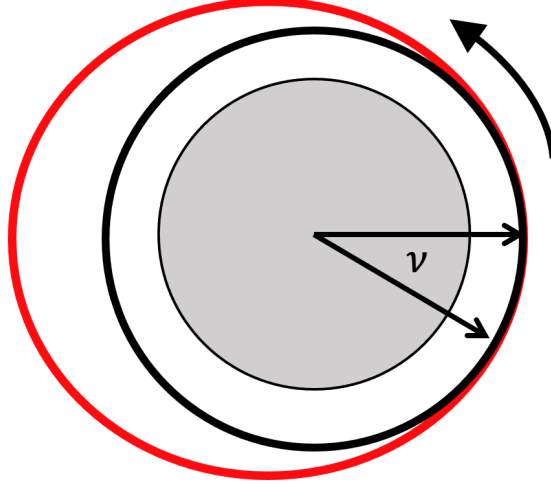


**Fig. 6 Phasing Maneuver**

same, but the change in true anomaly is positive for one and negative for the other. While effective at reducing the required fuel, it also requires twice the amount of follow-on collision detection. Certain rule-sets may find that limiting maneuvers to a single satellite is more effective overall.

## F. Station Keeping

Constellations often have strict requirements in their orbital elements to maintain a prescribed level of Earth ground coverage. To accurately model the ideal designs of future populations, station keeping maneuvers are implemented to act against the deviations in inclination, semi-major axis, and right-ascension if applicable. Two-body propagation could be leveraged to freeze these elements, but the omission of drag, solar radiation pressure, and non-spherical gravitational effects in the propagator was considered an excessive loss in fidelity. The frame used to describe the velocity changes is the radial, in-track, and cross-track (RIC) frame and which is visualized in Figure 7. The radial component is derived from the satellite radius vector, and the cross-track direction is perpendicular to the orbital plane. The in-track completes the triad as the cross product of the cross-track and radial directions.

To determine how to best model station-keeping within the simulation environment, an analysis into the observed behavior of current active constellations was performed, gathered from publicly available TLE data from SpaceTrack<sup>†</sup>. The two largest constellations with satellites that have active propulsion systems are Starlink and OneWeb. The time-history of a representative OneWeb satellite's semi-major axis is shown in Figure 8, which was compiled from over one-hundred days of tracking data. The OneWeb station keeping occurs approximately every 20 days, and displays a gradual return to the nominal altitude over several days, i.e., not suggestive of a two-impulse maneuver, but is contained in a relative narrow altitude bounding box of just 60 meters. This behavior was emulated in the simulation by using similar maneuver and raising intervals and a series of frequent, low-impulse thruster firings.

<sup>†</sup>[www.space-track.org](http://www.space-track.org)

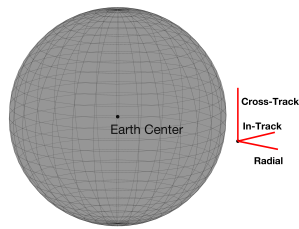


**Fig. 7 Radial, In-Track, Cross-Track Frame.**

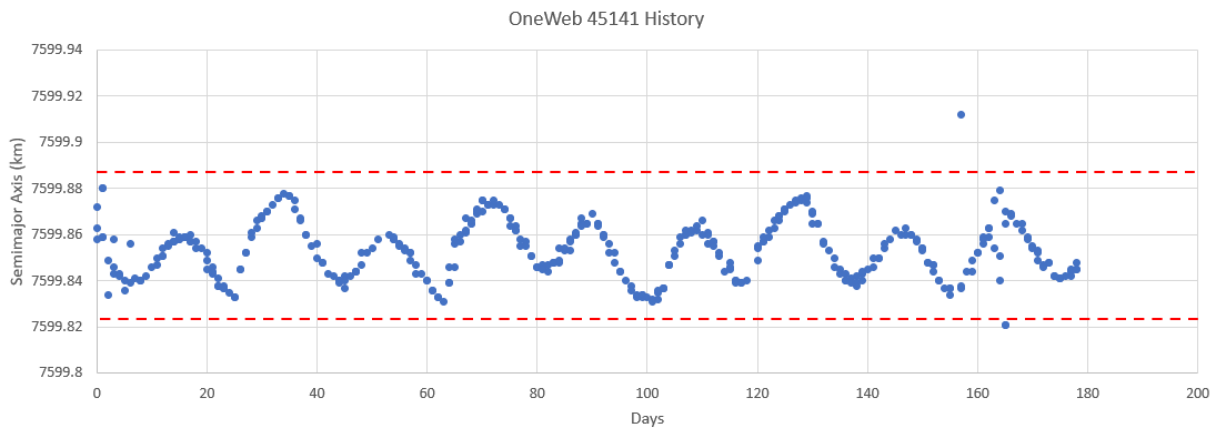


**Fig. 8 Observed Altitude Variations from 100 days of TLE data for a representative OneWeb satellite (NORAD ID 45141).**

Similar analysis was performed on the collection of approximately fifty Starlink satellites launched from early 2019 to late 2020, summarized in Table 1.

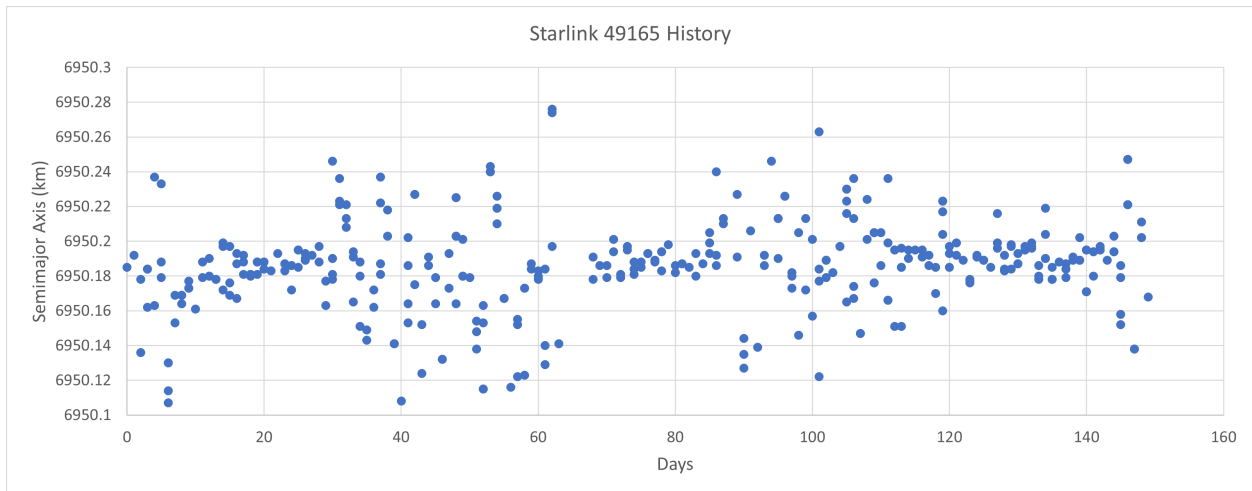


**Fig. 9 Data-Mined Starlink Altitude Maintenance.**

Launch Date(s)	SKF (days)	Orbit Window (km)
24 May 2019	13 ±10	±100
11 Nov 2019	7 – 14 ±20	±40
7 Jan 2020	7 ±5	±55
29 Jan 2020	12 – 14 ±5	±75
17 Feb 2020	6 – 9 ±15	±55
18 Mar 2020	4 – 6 ±20	±45
22 Apr 2020	7 – 14 ±10	±75
4 & 13 Jun 2020	6 – 11 ±15	±50
7 Aug 2020	5 ±5	±65
18 Aug 2020	6 ±5	±55
3 Sep 2020	4 ±5	±75
6 Oct 2020	9 – 12 ±10	±75
18 & 24 Oct 2020	4 – 6 ±10	±75
25 Nov 2020	6 ±10	±75

**Table 1 Starlink orbit and station keeping properties per launch group.**

The semi-major axis of a representative Starlink satellite is shown in Figure 9. The altitude maneuvering pattern is much less defined than those seen with OneWeb, but is important to note that the Starlink satellites are 650 kilometers lower in altitude than the OneWeb satellites. This decrease in altitude leads to a substantial increase in drag, and the wide variability observed implies that orbit maintenance may be conducted frequently in response to the drag and/or frequent conjunction avoidance actions. To freeze high-maintenance satellite orbits while limiting the complexity of the maneuver, it was determined to use daily maneuvers for Starlink for the current study. These have magnitudes on the order of millimeters per second, and are directly derived from the current altitude deviation from nominal. Daily maneuvers are not far-fetched for autonomous systems, and they are effective at quickly fixing deviations in constellation design. The equations used to calculate the magnitude and direction of the station keeping maneuvers originate from a Taylor series expansion of eccentricity and truncated by assuming near-circular orbits. [15] No dense, highly-eccentric constellations currently exist, so this approach is considered adequate for the constellations implemented.

$$\Delta a = \bar{a} - \hat{a} \quad (14)$$

$$\Delta v_I = \frac{n^2 \hat{a}}{2V} \Delta a \quad (15)$$

The deviation in semi-major axis at a point in time is defined as the current value subtracted from the design value. Eccentricity and inclination are also controlled, but require mean anomaly and argument of perigee to scale correctly. Both eccentricity and inclination correcting maneuvers are most efficient to perform near the apoapsis or periapsis of an orbit, so the magnitude of the correction is limited when not near either.

$$\Delta v_I = \frac{na\Delta e}{2 \cos M} \quad (16)$$

Worth highlighting is that the station keeping techniques implemented can be tailored to each constellation, e.g., in the current study, OneWeb and Starlink use different maneuvering policies. Undeployed constellations require assumptions about their behaviors, but this presents an opportunity to examine the relative number of events resulting from operator-specific norms of behavior.

### G. Orbit Raising and Decay

The simulation is intended to replicate not just the existence of constellations, but deployment and end-of-life behaviors as well. The satellite train in Figure 10, captured again from TLE data and consisting of a dozen OneWeb

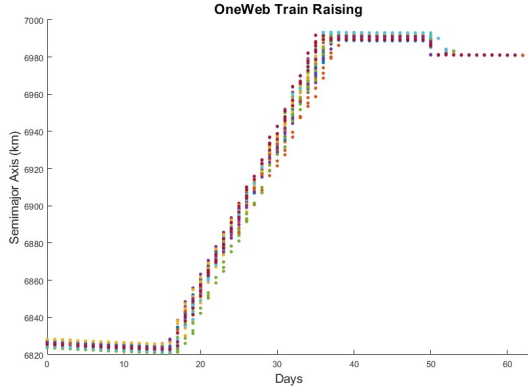


**Fig. 10 Data-Mined OneWeb Satellite Group Raising.**

satellites, demonstrates that orbit raising can take several weeks. Since the behavior is not suggestive of a quick impulse maneuver, a low-thrust imitation is required, similar to how station keeping is implemented, but extended to longer time frames. Using the constant thrust orbit raising algorithm as a starting point[16], the low thrust behavior is replicated as the sum of many small impulsive maneuvers separated by time-steps. New canonical units are introduced to simplify calculations. The distance unit is equal to the current satellite orbital radius.

$$DU = |r| \quad (17)$$

The time unit utilizes the gravitational parameter and the distance unit.

$$TU = \sqrt{\frac{(DU)^3}{\mu}} \quad (18)$$

The ratio of the final orbit radius to initial radius is calculated based the designs unique to each constellation, and the total commanded velocity can be calculated. Dividing by the length of the maneuver in terms of time-steps gives the velocity increase each time step.

$$V = \left(1 - \sqrt{\frac{\mu}{Ratio}}\right) * \frac{DU}{TU} \quad (19)$$

$$\Delta V = (t_{rise})/\delta t \quad (20)$$

The velocity added at each time step is the total velocity divided by the number of time steps required. For example, raising a satellite for thirty days with two-minute time steps requires 21,600 impulsive maneuvers. A sample case is shown for a 30 day burn with a 175-kilometer altitude raise.

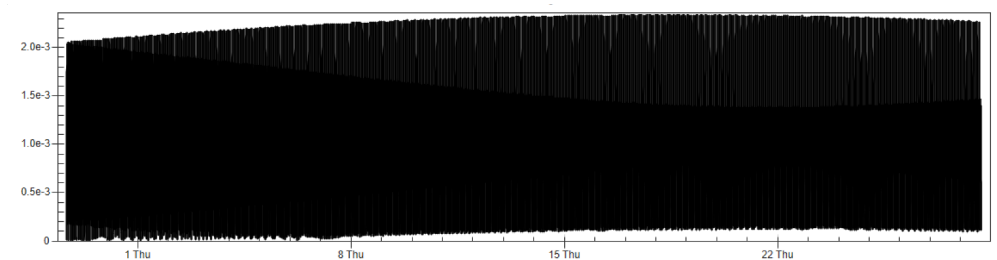


**Fig. 12 Simulated Eccentricity Evolution.**

The sample satellite successfully raised its semi-major axis by 175 kilometers as demonstrated in Figure 11 while the eccentricity never exceeds 2.0E-03 for the duration of the maneuver in Figure 12 This particular method of orbit raising is not universal, and variations in orbit raising is implemented specific to each constellation as an additional level

of fidelity, and again the impact of changing the assumed industry norm provides an image of possible best-practices. In Figure 10, all OneWeb satellites initiated their ascent simultaneously and exceeded the destination orbit. The inferred purpose for overshooting the altitude is to allow for phasing and insertion into the intended orbit. Starlink satellites take a slightly different approach, and use a low-altitude staging orbit and have each satellite raise at a different time to insert into the target orbit. This is illustrated along with the eccentricities in Figure 13, which is a compilation of a group of Starlink satellites launched and deployed over a six-month time frame starting the September 2020. The length of time that satellites are staged at the parking altitude is likely to allow gravitational precession to adjust orbital right-ascension and create multiple satellite planes from a single launch. At the designated time for orbit raising, the altitudes increase in a similar way to the simulated example in Figure 11, but the eccentricities that the Starlink satellites maintain are a factor of two smaller in magnitude than the OneWeb satellites. With finer treatment of the simulated maneuver flight path angle, this discrepancy will be corrected. To compare different techniques of orbit-raising, a flag is added to the satellite meta-data to indicate if a satellite is currently rising to a destination orbit. The efficacy of a particular strategy may be compared to other durations or altitude changes purely by the number of risky events that occur during the period of transition.

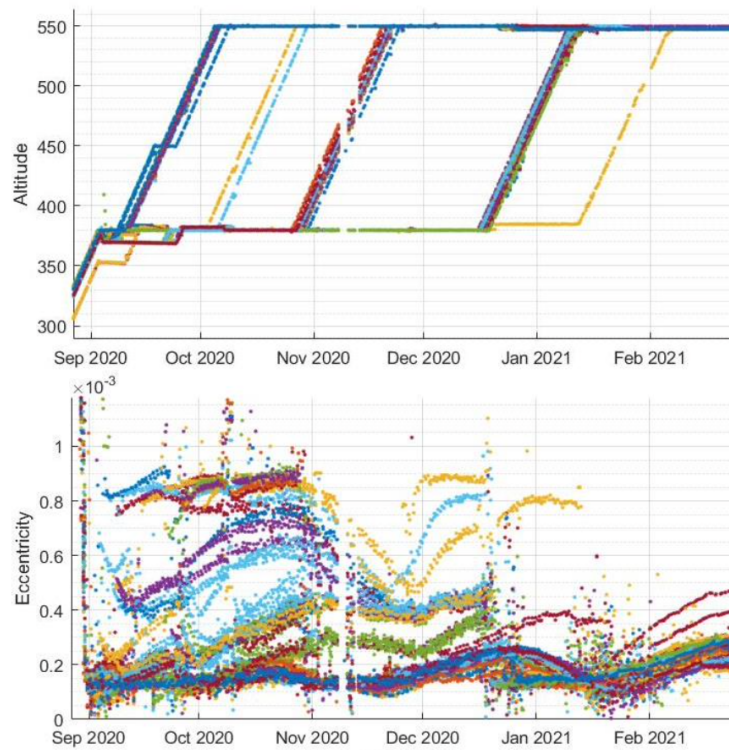


**Fig. 13 Data-Mined Starlink Satellite Raising.**

Similarly, typical methods to retire satellites was also examined. In Figure 14, plots of TLE data from Starlink satellites at their end-of-life show that they nominally descend first to a 400-kilometer altitude over the 3 months, followed by another descent to 350 kilometers leading to re-entry within the month. However, this did not occur in all cases, as several satellites decayed over the course of 3 to 4 years from a near 500 kilometer altitude. This extended de-orbit time-frame increases the likelihood that they will collide with other RSOs. For this reason, a decay failure percentage was implemented as a relevant input variable to model constellation end-of-life strategies and to explore acceptable rates of failure for varying operating altitudes. This requires the satellite metadata contain an additional tag describing whether or not it is in the process of deorbiting.

#### **IV. Verification and Validation**

To credibly determine rule-set recommendations, the simulation environment must realistically represent the conjunction frequency and Pc values currently represented in CDM data-sets. This was accomplished by examining the

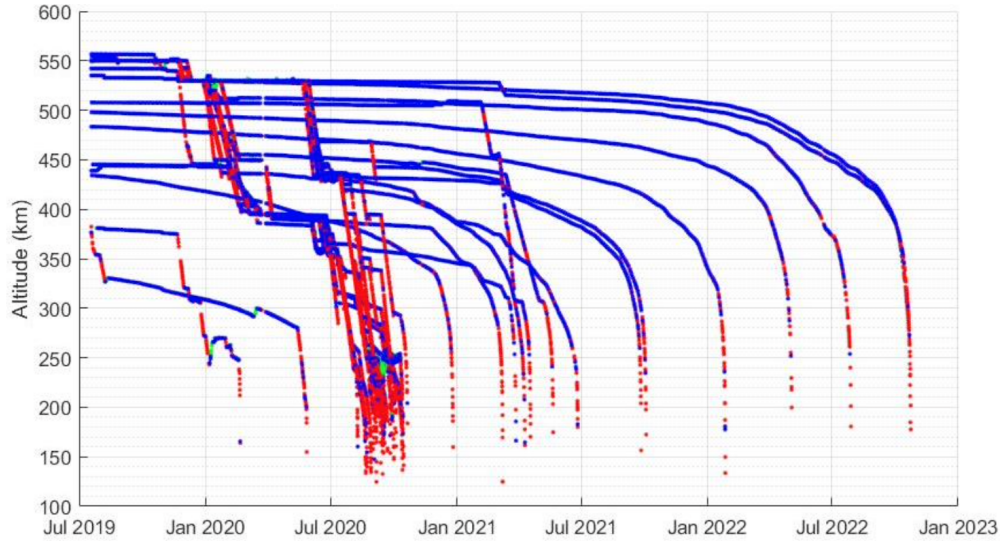


**Fig. 14 Starlink end-of-life altitude profiles plotted from TLE data.**

public CDMs provided by SOCRATES [17] and internal data provided by NASA’s CARA group. The former offers a shorter-term propagation validation, while the latter focuses more on event frequency than reproducing particular events.

### A. SOCRATES

SOCRATES is an online tool hosted by CelesTrak that predicts pending conjunctions three times a day for most active satellites. The exception is intra-constellation events, which constitute two-thirds of the number of weekly events. To correctly compare the simulation output to SOCRATES, the following operational assumptions are applied. Each SOCRATES computation covers a week of CDMs using public TLE data, and the screening distance for probability calculation is 5 kilometers. The general trend for recording events is a  $P_c > 1E-8$ , and all intra-constellation events are ignored to speed computation. As bulk downloads of SOCRATES CDMs are available with each new set of predictions, rapid comparisons can be made frequently. The implemented  $P_c$  calculation is Alfano’s method for maximum  $P_c$  utilized by SOCRATES, an algorithmic approach to covariance tuning that iterates the uncertainty magnitude to extract the highest possible  $P_c$ . [18]

The SOCRATES predictions are compared to simulation results using Figure 15 for early February and Figure 16 for late June. The SOCRATES data-set currently predicted approximately 55,000 collisions per week at a  $P_c > 1E-08$ . The simulation under-predicts for increasingly lower levels of risk, but the predictions level out for nearly actionable  $P_c$ s  $> 1E-06$ . The best guess for this discrepancy is the use of more accurate combined hard body radius values rather than typically oversized estimates derives from Radar Cross Section (RCS) estimates. In a scheme that iterates uncertainty, a smaller combined hard body radius will not benefit from the inflation of  $P_c$  as much as a larger radius. There is also an added difficulty correctly labeling satellites as operational for operations as up-to-date as SOCRATES, and thoroughly verifying the operating status of satellites will create latency between estimated operational status and SOCRATES assumed status.

Because SOCRATES generates these results three times a day, the comparison of rates can be repeated on a consistent basis. Generally, the number of events detected with the current catalog should be between 50,000 and 60,000, and the total number of events with  $P_c > 1E-5$  should be comparable. This particular  $P_c$  was chosen because it is the conservative side of industry-standard, actionable  $P_c$ s. Agreement at lower values is of less practical significance.

### B. NASA CARA

The second data-set utilized for the purpose of verification is an internally maintained NASA CARA history of notifications spanning nearly a year (January 2022 to November 2022) for 56 active NASA assets. Several entries may exist for the same encounter as the warning creation date approaches the estimated TCA, and the subsequent covariance for each is updated as measurements are gathered. For each notification, the 20-meter combined hard body radius

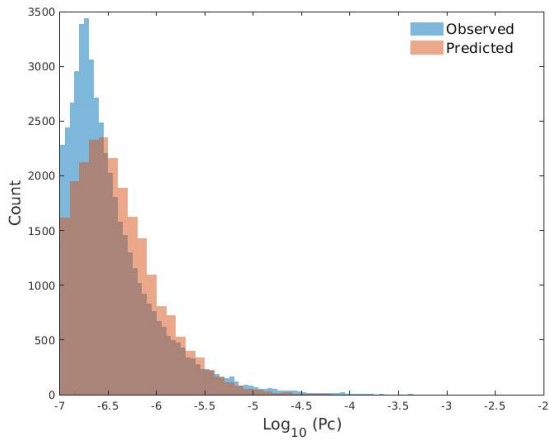


**Fig. 15 Simulation versus SOCRATES Predictions, Feb 4th.**

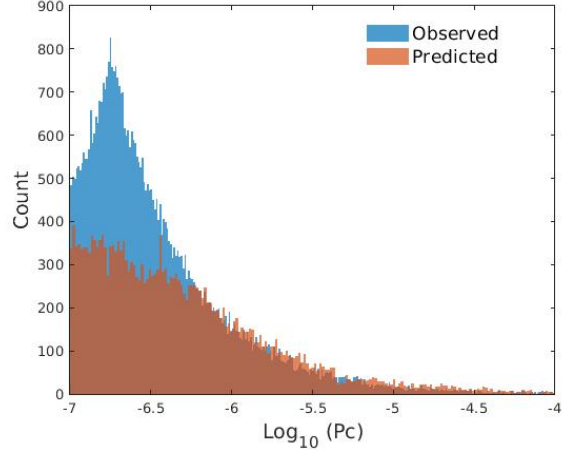


**Fig. 16 Simulation versus SOCRATES Predictions, June 21st.**

assumption is used for trend comparisons. In contrast to the Pc maximization that SOCRATES uses to manipulate the number of predicted events, this data-set allows the opportunity to examine how a covariance scaling factor may be applied to adjust the number of predicted events to a more realistic frequency.

The method of using TLE histories to estimate orbital covariance was found to slightly over-estimate the uncertainty used in creating the notifications, leading to dilution region events. [19] Just as Pc is the geometric intersection of two covariance ellipsoids, diluted covariances are over-inflated ellipsoids. The fact that position covariance is not symmetric across RIC axes implies the percentage of ellipsoid intersection does not increase at the same rate as ellipsoid volume. In short, if covariance values are too large, the corresponding probability of collision will decrease and high-risk events may be missed.

Data-mining all events with a Pc > 1E-04 with the assumption of a combined hard body radius of 20-meters, the rate of encounters per satellite was found to be 0.9 per day. Over the course of a month, the NASA CARA data set suggests the number of events should nominally be between 25 and 28. To study the effect of a varying scale factor, an expanded catalog of 28,000 objects with a screening distance of 25 kilometers was simulated for a year. In post-processing, the average number of events encountered by NASA assets normalized by the number of months per year was used to create Figure 17.

Generally, larger scale factors are less predictable in their detection rates, and scale factors as low as 0.2 produced events at an acceptable rate. Scale factors between 0.2 and 0.5 were determined to be the most consistent scale factor to use, with a default value of 0.3 used for the simulation case studies in section VI. From a geometric standpoint, the volume of an ellipsoid involves the multiplication of the three principal axis lengths.

$$V = \frac{4}{3}\pi r_1 r_2 r_3 \quad (21)$$

The length of each principal axis in matrix form is the square root of each diagonal element. Therefore, the multiplication by a scalar adjusts the uncertainly ellipsoid volume non-linearly as they depart from unity. For example a scale factor of 0.8 adjusts volume by nearly the same amount, 0.716, but dividing uncertainty by an order of magnitude reduces volume by a factor of thirty. This explains in part why the left-hand side of Figure 17 appears to decay exponentially.

### C. Historical LEO Distributions

CARA divides LEO into three altitude ranges designated as LEO 1, LEO 2, and LEO 3.[20] The upper limits on altitude are 500, 750, and 1400 kilometers respectively. Figure F-1 from the NASA Spacecraft Conjunction Assessment and Collision Avoidance Best Practices Handbook illustrates the notional distribution and annual frequency of conjunction events within these three altitude ranges. Assuming a 20 meter hard body radius, one would expect about 600 1E-7 events annually in LEO 1 and 400 in LEO 2 and LEO 3. For Pc > 1E-4, all regions should expect around 20 events annually. For 2 meters, approximately 100 1E-7 events and a single 1E-4 event is expected. Attempts to

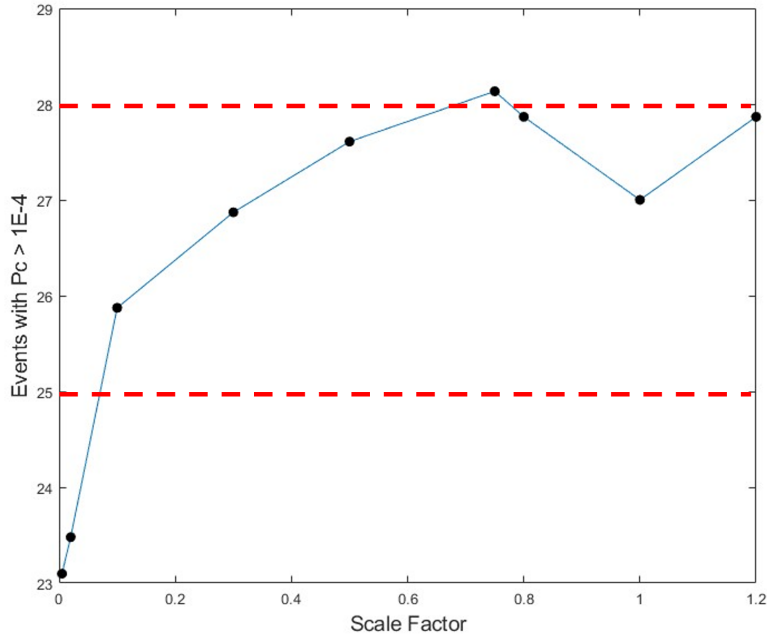


**Fig. 17 Simulated NASA Assets Event Frequency.**

reproduce this is shown in table 3, as well as the 2 meter hard body radius rates. For 2 meters, approximately 100  $1E-7$  events and 1  $1E-4$  event are expected.

Pc and HBR	LEO 1	LEO 2	LEO 3
1E-4, 2 meters	1	1	1
1E-7, 2 meters	100	100	100
1E-4, 20 meters	20	20	20
1E-7, 20 meters	600	400	400

**Table 2 Average historical rates of conjunction events per LEO zone, as determined by CARA.**

Pc and HBR	LEO 1	LEO 2	LEO 3
1E-4, 2 meters	0	0	0
1E-7, 2 meters	54	117.41	98.89
1E-4, 20 meters	4.36	14.44	14.11
1E-7, 20 meters	521.73	552.89	433.33

**Table 3 Simulation Results.**

Examining the results, the frequencies derived are roughly in-line for LEO 2 and LEO 3, but slightly under-reporting for LEO 1. One possible reason is under-sampling, as this contained the fewest number of tracked assets.

## V. Performance

The performance of the simulation is dependent on the number of satellites,  $P_c$  thresholds, and maneuver strategies. Utilizing 24 cores, propagating and detecting collisions for the current catalogue for a year requires around 4 to 5 hours.

## Current Active Population

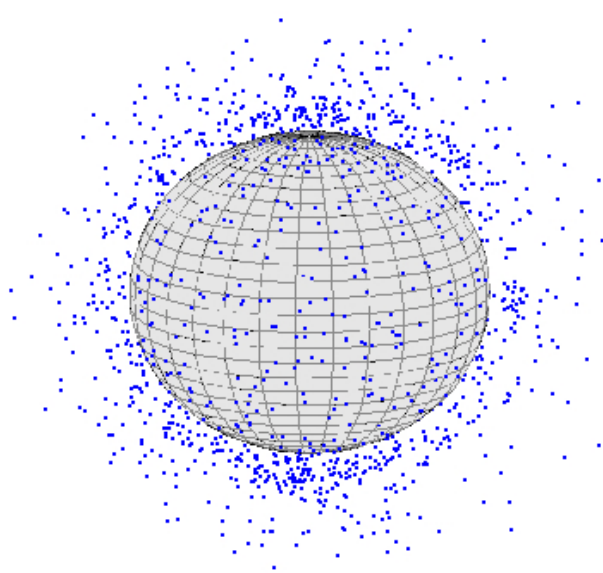


Fig. 18 Active Catalog.

## Constellations Added

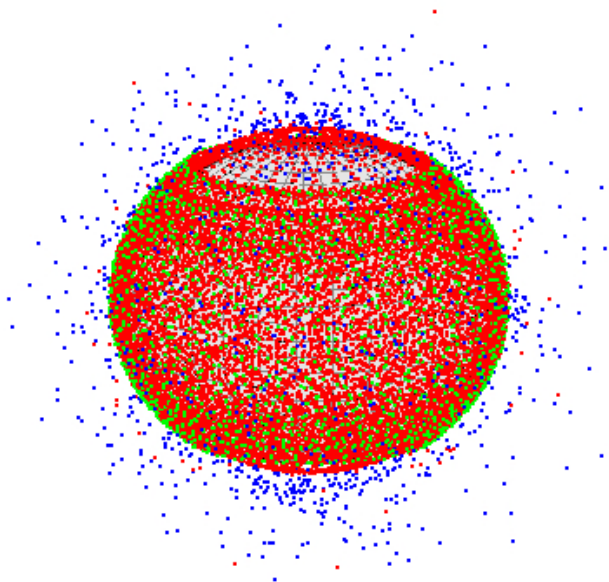


Fig. 19 Simulated Future Catalog.

For catalogues of over 50,000 active satellites, a year of simulation requires 12 hours of wall-time. This enables a wide variety of guidelines to be compared in a reasonable time-frame while also remaining up to date on industry standards.

## VI. Case studies

A year-long example case was used as an example run. The first included the space population on April 2nd, 2023, as captured by SpaceTrack. The best-estimate radii provided by NASA CARA are used for the hard body radius, a 25-kilometer spherical screening volume, and Chan's method for  $P_c$  calculation. Only operational satellites were modeled as primaries, making each iteration of collision detection checks 5,800 operational satellites against 25,000 objects. The wall-clock run time for this case, on 24 processors, was just four hours and three minutes. Just over one-million encounters were detected at a significance of  $1E-7$ , and 1,600 at  $1E-4$ . For 467,000 encounters, both satellites were active, and the remainder had only a single active satellite. Particularly large objects like the International Space Station (ISS) received 1638 notifications alone. The volume expected of a 20 meter hard body radius discussed previously was 600 annually at the  $1E-7$  level, so 1,600 is consistent with the ISS being slightly over 100 meters in size.

In addition to the space population of February 4th, 2023 in 18, a denser space population of 30,000 projected Starlink satellites and 4,000 Kupier satellites in Figure 19 were simulated for a first glance at future pollution risks. The number of events at  $P_c > 1E-4$  for the year, excluding intra-constellation events, was 15 times larger at a total of 24,400. When including the number of intra-satellite constellation events we quickly discover millions of events and detection is considerably slowed down, from the 7 hours of the previous run to roughly 15 hours total. It is assumed that constellations are able to self-manage their own collision avoidance, so the intra-constellation events are omitted from the final statistics. With the inclusion of maneuvers, only six-percent of maneuvers were the result of non-constellation encounters, implying an additional burden of nearly 17-times more maneuvers per satellite on average in this space population. The remaining 94-percent of maneuvers involved just one satellite from a constellation, while intra-constellation encounters were assumed to be resolved. Shared maneuvers typically involved velocity changes on the order of one meter-per-second for each satellite each, while single-satellite maneuvers were more efficient overall with only a 25-percent increase in total velocity change.

## VII. Conclusion

We have introduced a simulation environment to examine the performance of rule-sets in the context of both current and future space populations. Current space populations are used as a source of validation, and the predictions generated calibrated by both the private and public catalogues are consistent with observed conjunction frequencies. With this verification, simulations of future space populations may be performed with the confidence that the results are representative of reality.

The implementation of maneuvers has been introduced to serve two purposes. A pair of phasing maneuver are implemented to return satellites to their operational orbits while minimizing the change in velocity, and the use of satellite meta-data is introduced to allow maneuver assignment on a contextual basis. Factors such as age, usage type, nation of origin, mass, and operating status present parametric method of designating priority each simulation. An equivalent range of outputs are supplied to compare techniques such as the change in velocity required, the frequency of maneuvers, the total number of high-risk encounters, and the number of events due uniquely to orbit-raising, end-of-life, and the additional burden constellations leave on existing infrastructure.

Historical orbit data of Starlink and OneWeb provided an empirical basis upon which to create generalized functionality. Orbit raising is observed for both Starlink and OneWeb examples, and an algorithmic replication in demonstrated through thousands of small, impulsive burns, and the algorithm is abstracted enough to apply to all LEO constellations. The Starlink station keeping history in investigated reflects the need for frequent adjustments, so equations for altitude and eccentricity maintenance on a daily basis have been introduced. Finally, the end-of-life management of a Starlink fleet reflected both the use of staging and the non-trivial possibility of failure prior to mission completion.

Risk is described in a number of different ways that all contribute to space sustainability. The acceptable risk threshold is tuned to adjust the number of maneuvers undergone while simultaneously increasing the likelihood of a collision event. With increasingly frequent events, the total probability of collision is computed, and when the likelihood of a collision reaches 99.999 percent, the number of detected collisions will increase. Alongside the number of collisions likely to occur within a given time and environment combination, the debris generation is characterized. In the characterization of fragmentation behavior, the potential debris creation for a modern catalog over a year is examined, and the majority of collisions that might occur at the present are deemed catastrophic due to the energy of impact. In 0.8 percent of cases debris fragments may exceed 200,000 in number, and exceed 100,000 pieces in the majority of collisions that exclude intra-constellation events. Combined, these metrics represent the average rate of debris creation for a combination of maneuver guidelines and space population.

Future work will explore a range of rule-sets to find points of balance between commercial applications, scientific satellites, and overall environmental stability. Work towards accurate imitations of industry norms in other aspects such as risk thresholds and maneuver strategies to improve the simulation environment fidelity. Constellation examples of orbit raising and retirement have been examined, and efforts will be made to determine best-practice behaviors depending on the space population.

## Acknowledgments

This research was supported in part through research cyber-infrastructure resources and services provided by the Partnership for an Advanced Computing Environment (PACE) at the Georgia Institute of Technology, Atlanta, Georgia. This work was partially supported by NASA (Grant 80NSSC22K0986). Schweiger, G., Gunter, B.C., Murphy, T., " A Survey and 3LE Generation Model of Megaconstellations in the Future LEO Environment," Submitted to the AIAA SciTech Conference, Orlando, FL, January 8-12, 2024.

## References

- [1] Oltrogge, D. L., "The contributions of commercial best practices to the global space governance continuum," 2020.
- [2] Macke, R. J., Gunter, B. C., Borowitz, M., and Birch, M., "Analysis of Potential Collision Maneuver Guidelines for Future Space Traffic Management," *Paper AAS*, 2021, pp. 21–717.
- [3] Borowitz, M., Gunter, B. C., Birch, M., and Macke, R. J., "An investigation into potential collision maneuver guidelines for future Space Traffic Management," 2021.
- [4] Andrişan, R. L., Ioniţă, A. G., González, R. D., Ortiz, N. S., Caballero, F. P., and Krag, H., "Fragmentation event model and assessment tool (FREMAT) supporting on-orbit fragmentation analysis," *7th European Conference on Space Debris*, 2016.

- [5] Cimmino, N., Isoletta, G., Opromolla, R., Fasano, G., Basile, A., Romano, A., Peroni, M., Panico, A., and Cecchini, A., “Tuning of NASA standard breakup model for fragmentation events modelling,” *Aerospace*, Vol. 8, No. 7, 2021, p. 185.
- [6] Burgis, S., Rohrmüller, L., Michel, M., and Bertrand, R., “Simulation of satellites and constellations for the assessment of collision avoidance operations,” *CEAS Space Journal*, 2022, pp. 1–16.
- [7] Healy, L. M., “Close conjunction detection on parallel computer,” *Journal of Guidance, Control, and Dynamics*, Vol. 18, No. 4, 1995, pp. 824–829.
- [8] Zhang, Y., Li, B., Liu, H., and Sang, J., “An analysis of close approaches and probability of collisions between LEO resident space objects and mega constellations,” *Geo-spatial Information Science*, Vol. 25, No. 1, 2022, pp. 104–120.
- [9] 18th, and 19th Space Defense Squadron, *SFS Handbook For Operators VI.7.pdf*, April 2023.
- [10] Alarcón Rodríguez, J., Martínez Fadrique, F., and Klinkrad, H., “Collision Risk Assessment with aSmart Sieve’Method,” *Joint ESA-NASA Space-Flight Safety Conference*, Vol. 486, 2002, p. 159.
- [11] Mashiku, A. K., and Hejduk, M. D., “Recommended Methods for Setting Mission Conjunction Analysis Hard Body Radii,” *2019 AAS/AIAA Astrodynamics Specialist Conference*, 2019.
- [12] Hall, D. T., “Implementation recommendations and usage boundaries for the two-dimensional probability of collision calculation,” *2019 AAS/AIAA Astrodynamics Specialist Conference*, 2019.
- [13] Chan, K., “SPACECRAFT COLLISION PROBABILITY FOR LONG-TERM ENCOUNTERS,” 2020.
- [14] Hejduk, M., Laporte, F., Moury, M., Newman, L., and Shepperd, R., “Consideration of Collision” Consequence” in Satellite Conjunction Assessment and Risk Analysis,” *International Symposium on Space Flight Dynamics*, 2017.
- [15] Vallado, D. A., *Fundamentals of astrodynamics and applications*, Vol. 12, Springer Science & Business Media, 2001.
- [16] Alfano, S., and Thorne, J., “Constant-Thrust Orbit-Raising Transfer Charts,” 1993, p. 23.
- [17] Kelso, T. S., and Alfano, S., “Satellite Orbital Conjunction Reports Assessing Threatening Encounters in Space(SOCRATES),” *Advances in the Astronautical Sciences*, Vol. 120, 2005, pp. 317–326.
- [18] Alfano, S., “Relating position uncertainty to maximum conjunction probability,” *The Journal of the Astronautical Sciences*, Vol. 53, 2005, pp. 193–205.
- [19] Hejduk, M. D., Snow, D., and Newman, L., “Satellite conjunction assessment risk analysis for “dilution region” events: issues and operational approaches,” *Space Traffic Management Conference*, 2019.
- [20] Krage, F. J., “Nasa spacecraft conjunction assessment and collision avoidance best practices handbook,” Tech. rep., 2023.